Underwater multi-view three-dimensional imaging with passive sensing

Bahram Javidi, Robert Schulein, and Myungjin Cho
Dept. of Electrical and Computer Engineering, U-2157, University of Connecticut, Storrs, CT USA 06269-2157
Bahram@engr.uconn.edu

ABSTRACT

In this keynote address paper, an overview of multi-view three-dimensional (3D) imaging with passive sensing for underwater applications is presented. The 3D Synthetic Aperture Integral Imaging (SAII) technique is adapted for underwater sensing. The change in apparent object distance caused by the refractive index of water must be accounted for in computational 3D image reconstructions. An experimental environment with objects in water and SAII system in air or water is presented. Experimental results are presented to demonstrate the ability of the underwater 3D SAII system.

Keywords: Integral Imaging, 3D Imaging, Underwater Imaging

1. INTRODUCTION

Multi-view three-dimensional (3D) imaging systems [1-4] have been a promised next generation imaging technique. Integral imaging (II), which was first proposed by G. Lippmann [5, 6], has some advantages over other 3D imaging systems. In general, stereoscopic methods such as binocular stereogram need special glasses to observe the 3D image and also have limited viewing points, unidirectional parallax, and visual fatigue. In holography, the coherent light source is required to obtain the 3D image. However, II has continuous viewing points, full parallax, and less visual fatigue. II is an attractive method to utilize commercial inexpensive imagers because incoherent light is used for illumination. Therefore, the natural 3D scene can be acquired. In this keynote paper, an overview of multi-view 3D imaging with passive sensing for underwater applications is presented [7].

In this paper, we describe Synthetic Aperture Integral Imaging (SAII) systems [8-9]. SAII is a recording method of II. It can be used for an underwater environment. In conventional II systems, a lenslet array is used to collect multi-view images onto a single sensor plane [10]. It is useful for real-time 3D applications, but it has some drawbacks; low lateral and longitudinal resolution, crosstalk between neighboring elemental images, low depth-of-focus, and a pseudoscopic problem. High resolution image sensor or time-multiplexed sensing like Moving Array-Lenslet Technique (MALT) is required to enhance the resolution and depth-of-focus [11]. An optical barrier is needed to remove image crosstalk [10, 12]. Also, a pseudoscopic-to-orthoscopic (P/O) conversion should be implemented to observe the correct 3D image [10, 12]. However, it spends a lot of time and costs. Therefore, to overcome these problems, SAII was introduced because each multi-view image is captured using an entire imager lens and sensor. In SAII, the resolution of each elemental image is the same as that of the single imager. Figure 1 illustrates the optical recording process of an SAII system.

In computational reconstruction for SAII, the 3D image can be reconstructed by back projecting multi-view images through a virtual lens or pinhole array. The parameters of the virtual lens or pinhole array used in reconstruction should be the same as that used in pickup. We use a computational volumetric reconstruction algorithm to obtain the 3D reconstructed image [13]:

$$I(x,y,z_r)=\frac{1}{KL}\sum_{k=0}^{K-1}\sum_{l=0}^{L-1}I_{kl}\left(x+\frac{S_k k}{M_r},y+\frac{S_l l}{M_r}\right), \tag{1}$$

Enabling Photonics Technologies for Defense, Security, and Aerospace Applications VI, edited by Michael J. Hayduk, Peter J. Delfyett Jr., Andrew R. Pirich, Eric J. Donkor, Proc. of SPIE Vol. 7700, 770002 · © 2010 SPIE
CCC code: 0277-786X/10/$18 · doi: 10.1117/12.852985

where x and y are the index of pixels for each elemental image, K and L are the total number of respective horizontal and vertical perspective images, and S_k and S_l denote the respective horizontal and vertical physical offsets between perspective imaging positions. In Eq. (1), M_r is the magnification of the reconstruction plane at distance z_r away from the SAII array and is defined by $M_r=z_r/f_r$, where f_r is the focal length of the virtual pinhole/lens array. As shown in Fig. 2, objects will appear in focus at a reconstruction plane related to the original object plane, z_{obj}, and will appear blurred and out of focus at other reconstruction planes.

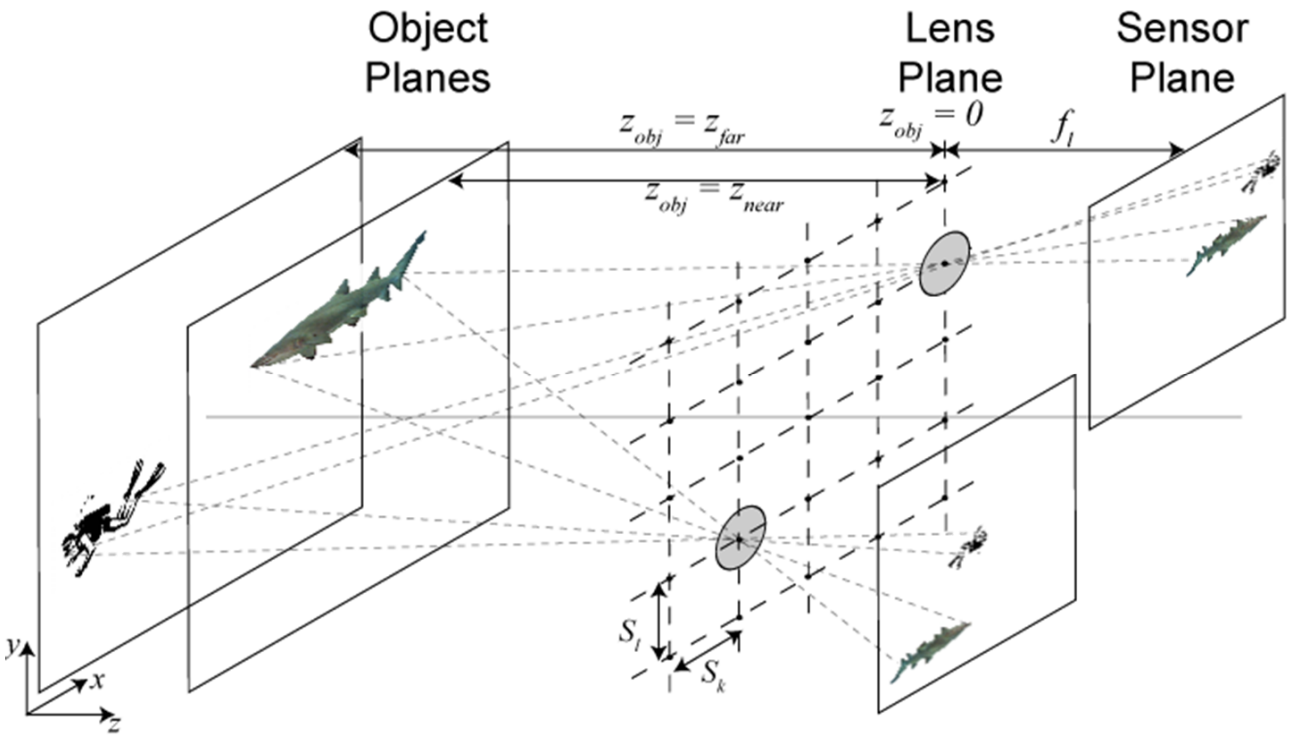

Figure 1. Optical pickup process for a Synthetic Aperture Integral Imaging (SAII) system with imagers distributed on a lateral grid. Either a camera is translated between or a camera array is distributed along a lateral grid. An incoherent 2D intensity image is taken from each imaging point. Based on the relationship between an object's position in space and the imager's position on the lateral grid, the object will be imaged onto a different part of the imager. Notice the relative different positions each object is imaged onto in the two different imaging positions.

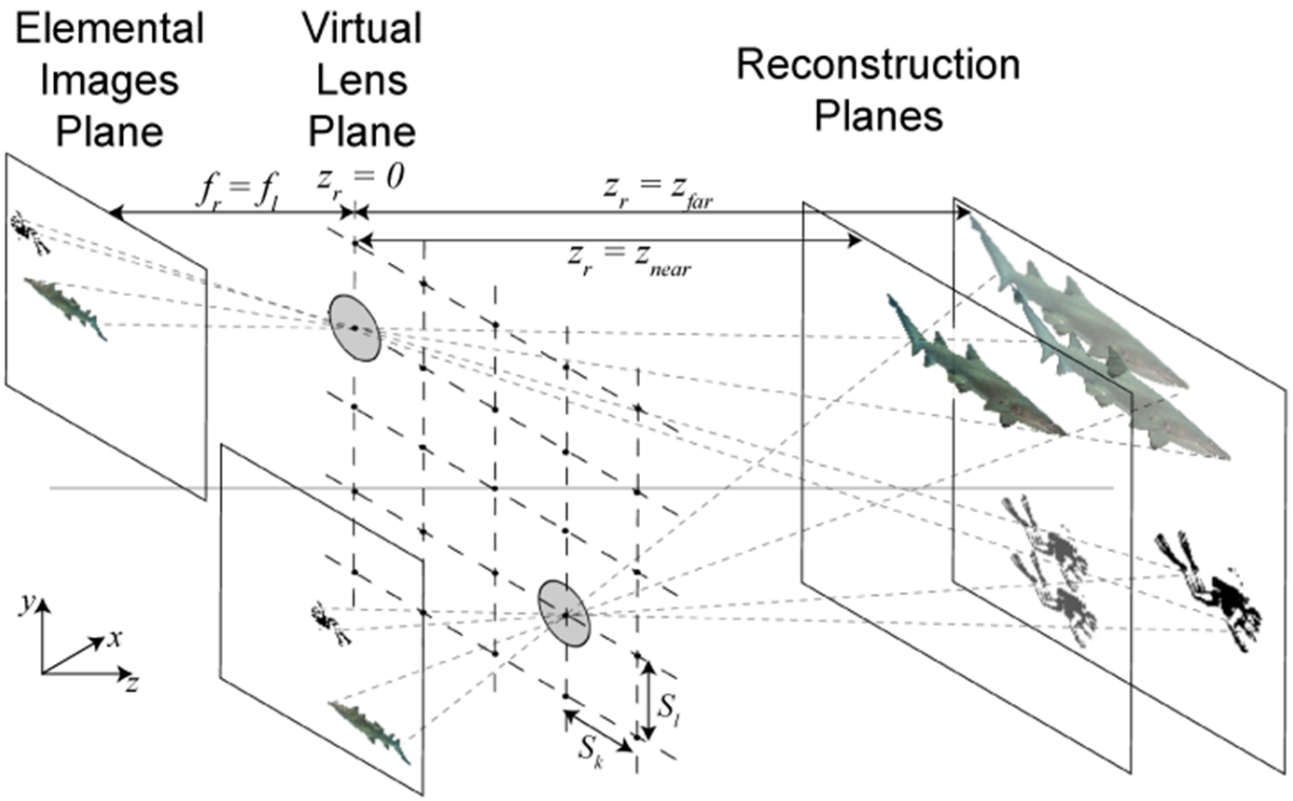

Figure 2. 3D computational reconstruction process for SAII. Each perspective image is inversely propagated through a virtual lens/pinhole with parameters similar to the pickup process. Reconstruction images are formed by measuring the superposition of all perspective images back propagated through the virtual lens/pinhole array onto a plane at an arbitrary distance from the array. Objects will appear in focus at reconstruction planes that correspond to the plane the object was in during the pickup process and will appear out of focus at other reconstruction planes.

Because each multi-view image should cover the entire object for best performance, the size of the synthetic aperture should be considered [4, 9]. Therefore, the maximum size of the synthetic aperture, $D_{\max}$, which is equivalent to the spread between the furthest imagers (S_kK nd S_LL for the respective horizontal and vertical spaced perspective imagers), will be limited by the pickup lens' field of view (FOV) and the object's lateral size, R, and distance from the SAII array:

$$D_{\max} = 2z_{obj} \tan\theta_{HFOV} - R\,, \tag{2}$$

where θ_{HFOV} is the angle representing the lens' half FOV. When object is non square, horizontal and vertical maximum synthetic aperture size may be different from each other. In general, the horizontal size of imager is larger than the vertical size of imager.

SAII technique can be applied to many applications: 3D object recognition [14-16], 3D object tracking [17], free-view reconstruction [18, 19], and profilometry [20]. All of these applications have done in the presence of heavy foreground occlusion that would completely block the background target in conventional 2D imaging. In this keynote paper, we adapt SAII to underwater imaging. There have been previous studies into underwater imaging systems using LIDAR [21], and combination 2D imaging and sonar [22] but these have done in 2D image space. In this keynote paper, we

overview our previous work and demonstrate how to adapt an SAII system for the underwater imaging scenario. The scenario involves an SAII system in air recording objects that are in water. The modified reconstruction algorithms for underwater imaging are derived and experimental results are shown.

2. UNDERWATER INTEGRAL IMAGING

To reconstruct the underwater image, many optical effects such as wavelength-dependent absorption, scattering, dispersion, glare of water surface, and index of refraction variations should be considered [23, 24]. In this keynote paper, we only consider difference of refraction indexes between water (≈1.33) and air (≈1.00). We assume that an observer watches an underwater object from air perpendicular to water surface. The apparent object distance from water surface, z_{water}, is $z'_{water}=z_{water}/n_{water}$ [18]. Thus, the total apparent optical path length from observer to object is equal to the distance in air added to the apparent distance in water.

Using the total apparent optical path length from observer to object in an SAII system, the 3D reconstructed image at the correct object distance can be obtained. The computational reconstruction algorithm as shown in Eq. (1) is still valid for underwater imaging system but the magnification ratio, M_r, must be modified as follows:

$$M_r = \frac{z_{air} + \dfrac{z_{water}}{n_{water}}}{f_r}, \tag{3}$$

with z_{air} the physical in-air distance of the optical path, z_{water} the physical in-water distance of the optical path, n_{water} the index of refraction of water, and f_r the focal length of the lens. If n_{water} is estimated incorrectly, the reconstruction plane will be slightly different.

When image sensor is located perpendicular to the water surface, its FOV changes by $\theta_{HFOV}=\sin^{-1}(\sin\theta_{HFOV}/n_{\text{water}})$ due to difference of refraction indexes between water and air [18]. Due to variations of FOV and optical path length, the maximum size of the synthetic aperture changes as follows:

$$D_{\max} = 2\left(z_{air} + \frac{z_{water}}{n_{water}}\right)\tan\theta_{HFOV} - R, \tag{4}$$

where θ_{HFOV} is the lens' half field of view (FOV) in water and R is the lateral size of the object. Maximum performance of SAII system is decreased from Eq. (4). Therefore, the offset distance should be reduced to enhance the performance of SAII system in water.

3. UNDERWATER EXPERIMENTAL RESULTS

In this section, we present experimental results of an imaging scenario where the SAII system is simulated to be in water looking at a scene that is in water. This experiment shows the underwater SAII system can reconstruct 3D image with heavy occlusion. A scene was set up in a 10 gallon fish tank to simulate underwater SAII scenario. The SAII array was placed directly up against one side of the fish tank, reducing the in-air optical path distance to nothing and simulating an underwater SAII system. The scene consisted of a sign placed 230mm away from the SAII viewing window, a toy treasure chest at 340mm, a toy fish at 380mm, and a toy deep sea creature from 435mm to 495mm. The 10 gallon tank was filled completely with fresh tap water and illuminated from above with a diffuse incoherent lamp to simulate sun

light. A central 2D incoherent perspective image taken within the SAII system is shown in Fig. 3(a) and all of the figures within the scene can be clearly seen.

(a)

(b)

Figure 3. Objects used in Experiment. (a) Objects without occlusion in water, (b) Objects with occlusion in water

After taking a set of SAII images in clear water, foreground occlusion was added to the scene. This occlusion consisted of twigs and plastic foliage and was placed at ≈100mm away from the SAII viewing window. A central 2D incoherent perspective image taken within the SAII system of the occluded scene is shown in Fig. 3(b). As can be seen, some of the figures are partially occluded while others are completely occluded in this one perspective image.

An SAII data set was collected of the occluded scene by translating a single camera along a transverse x-y lateral 5mm x 5mm grid with the lens flush with the fish tank. Overall, 9 horizontal nodes and 7 vertical nodes were used for a total of 63 perspective images in a 40mm × 30mm synthetic aperture. This synthetic aperture was chosen such that all of the objects within the scene were completely imaged by each perspective image and $D_{\max}$ was maximized for optimum collection capabilities. A full frame 35.8mm × 29.9mm CMOS imaging sensor with 4,368 × 2,912 pixels and 8.2μm pitch was used with a f_l = 50mm focal length lens. The lens was stepped down to its smallest aperture to achieve the maximum depth of field and ensure that all objects would be in focus for each perspective image.

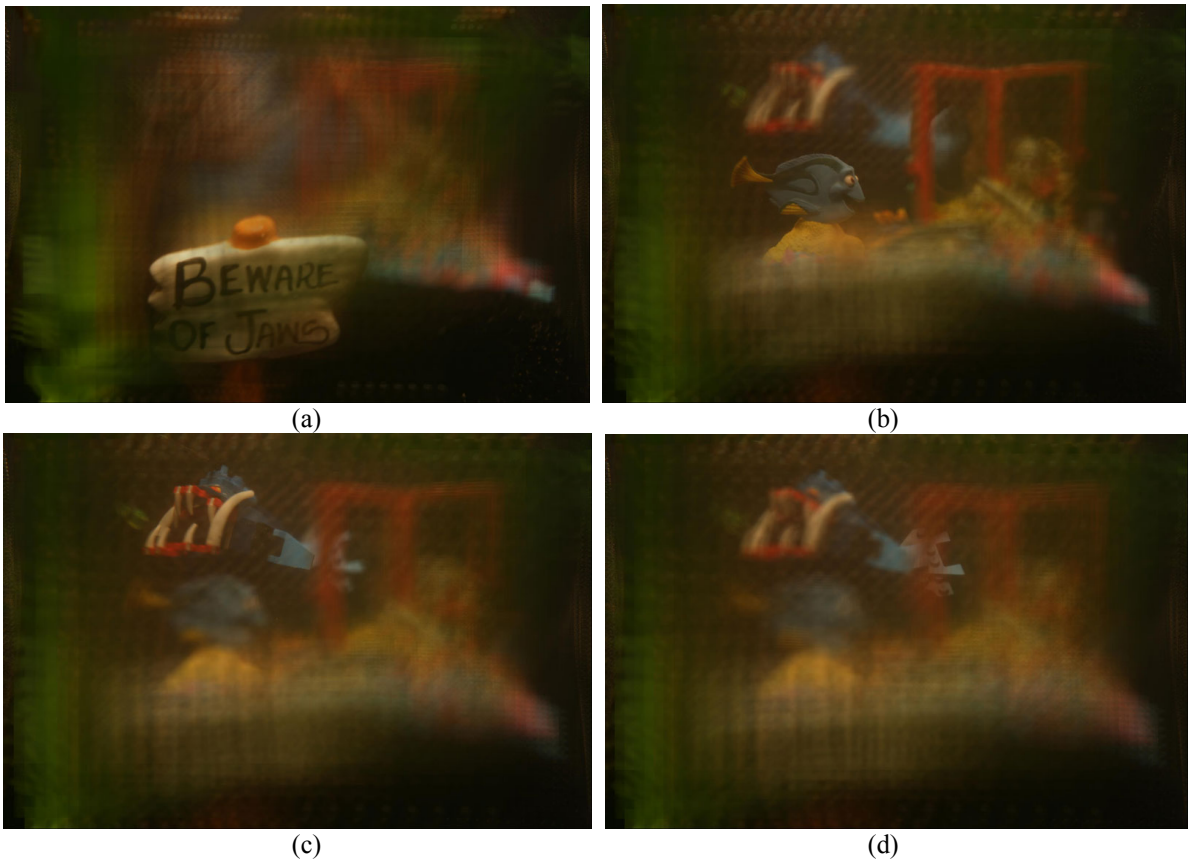

Figure 4. Experimental results. (a) 3D computational reconstruction at z = 230mm of the occluded scene, bringing the foreground sign into focus. The sign is almost completely occluded in the central 2D elemental image shown in Fig. 3(b). (b) 3D computational reconstruction of the occluded scene at z = 380mm, which brings the central toy fish into focus. (c) 3D computational reconstruction of the occluded scene at z = 440mm, which focuses on the jaw of the deep sea creature in the background. The deep sea creature was also heavily occluded in Fig. 3(b). (d) 3D computational reconstruction of the occluded scene at z = 480mm, which brings the tail of the deep sea creature into focus. The tail of the deep sea creature was occluded Fig. 3(b) but also in Fig. 3(a) by the midground treasure chest but now more detail comes into focus.

Because there was no in-air component to the optical path, Eq. (3) was reduced to $M_r=z_{water}/(n_{water}f_r)$ for reconstruction calculations. Because the glass of the tank was thin and perpendicular to the optical axis, its effects on path length and angle of view were negligible and therefore ignored. The index of refraction of water, n_{water}, was approximated to 1.33 and f_r was equal to the focal length of the lens used for acquisition, 50mm. Plane-by-plane reconstructions were performed on the acquired occluded data using Eq. (1) and (3). Reconstruction results at different planes are shown in Fig. 4(a-d).

As can be seen in Fig. 4(a-d), occluded objects come into focus at their correct reconstruction plane and appear blurry at other reconstruction planes. The objects are successfully seen through the occlusion that almost completely blocked them in Fig. 3(b). In this section, we showed the abilities of the adapted SAII system to work in a completely in-water environment that also contains heavy foreground occlusion.

4. CONCLUSION

In this keynote address paper, an overview of multi-view three-dimensional (3D) imaging with passive sensing for underwater applications was presented. Underwater 3D computational reconstructions were created by modifying traditional reconstruction techniques to account for the difference of refractive index between air and water. To verify the system performance, experimental results were shown for an underwater imaging scenario. The ability of the SAII system to reconstruct objects behind heavy occlusion in an underwater environment was shown.

REFERENCES

[1] Okoshi, T., [Three-Dimensional Imaging Techniques], Academic Press (1976).

[2] Benton, S., Ed., [Selected Papers on Three-Dimensional Displays], SPIE Press (2001).

[3] Javidi, B., Okano, F., and Son, J., Eds., [Three Dimensional Imaging, Visualization, and Display Technology], Springer (2008).

[4] Stern, A. and Javidi, B., "Three-dimensional image sensing, visualization, and processing using integral imaging," Proceedings of the IEEE 94(3), 591–607 (2006).

[5] Lippmann, M.G., "La photographie int´egrale," Comptes-rendus de l'Acad´emie des Sciences 146, 446–451 (1908).

[6] Sokolov, P., "Autostereoscopy and Integral Photography by Professor Lippmanns Method," Moscow State Univ. Press, Moscow (1911).

[7] Schulein, R. and Javidi, B., "Underwater Multi-View Three-Dimensional Imaging," J. Disp. Tech. 4, 351-353 (2008).

[8] Jang, J.-S. and Javidi, B., "Three-dimensional synthetic aperture integral imaging," Opt. Lett. 27, 1144-1146 (2002).

[9] Stern, A. and Javidi, B., "3-D computational synthetic aperture integral imaging (COMPSAII)," *Opt. Exp.* 11, 2446-2451 (2006).

[10] Okano, F., Hoshino, H., Arai, J., and Yuyama, I., "Real-time pickup method for a three-dimensional image based on integral photography," Appl. Opt. 36, 1598-1603 (1997).

[11] Jang, J.-S. and Javidi, B., "Improved viewing resolution of three-dimensional integral imaging by use of nonstationary micro-optics," Opt. Lett. 27, 324-326 (2002).

[12] Arai, J., Okano, F., Hoshino, H., and Yuyama, I., "Gradient-index lens-array method based on real-time integral photography for three-dimensional images," Appl. Opt. 37, 2034-2045 (1998).

[13] Hong, S.-H., Jang, J.-S. and Javidi, B., "Three-dimensional volumetric object reconstruction using computational integral imaging," *Opt. Exp.* 12, 483-491 (2004).

[14] Hong, S.-H. and Javidi, B., "Distortion-tolerant 3D recognition of occluded objects using computational integral imaging," Opt. Exp. 14, 12085-12095 (2006).

[15] Javidi, B., Ponce-Diaz, R., and Hong, S.-H., "Three-dimensional recognition of occluded objects by using computational integral imaging," Opt. Lett. 31, 1106-1108 (2006).

[16] Schulein, R., Do, C. M., and Javidi, B., "Distortion-tolerant 3D recognition of underwater objects using neural networks," JOSA A, 27, 461-468 (2010).

[17] Cho, M. and Javidi, B., "Three-dimensional tracking of occluded objects using integral imaging," Opt. Lett. 33, 2737-2739 (2008).
[18] Hwang, Y. S., Hong, S.-H. and Javidi, B., "Free View 3-D Visualization of Occluded Objects by Using Computational Synthetic Aperture Integral Imaging," *J. Display Technol.* 3, 64-70 (2007).
[19] Cho, M. and Javidi, B., "Free View Reconstruction of Three-Dimensional Integral Imaging Using Tilted Reconstruction Planes With Locally Nonuniform Magnification," J. Display Technol. 5, 345-349 (2009).
[20] DaneshPanah, M. and Javidi, B., "Profilometry and optical slicing by passive three-dimensional imaging," Opt. Lett. 34, 1105-1107 (2009).
[21] He, D.-M. and Seet, G., "Underwater LIDAR imaging in highly turbid waters," *Proc. SPIE*, 4488, 71-81 (2002).
[22] Glecker, A. and Pittner, A., "Multipurpose underwater imaging and ranging camera: Prototype system performance," *Proc. SPIE* 4039, 145-149 (2000).
[23] Glover, T., Harwood, G. E. and Lythgoe, J. N., [*A Manual of Underwater Photography]*, Academic Press, New York (1977).
[24] Mertens, L.E., [*In-Water Photography]*, Wiley-Interscience, New York (1970).